Hindawi
Modelling and Simulation in Engineering
Volume 2021, Article ID 5532276, 17 pages
https://doi.org/10.1155/2021/5532276

Research Article

Optimization of AL6061-T6 Tube End Forming Process Using Response Surface Method

Amr Shaaban and Adel M. Elsabbagh

Design & Production Engineering Dept. Faculty of Engineering, Ain-Shams University, Egypt

Correspondence should be addressed to Amr Shaaban; amr.ahmed@eng.asu.edu.eg

Received 16 January 2021; Revised 24 March 2021; Accepted 29 March 2021; Published 12 April 2021

Academic Editor: Angelos Markopoulos

Tube end closing is a metal forming process that replaces welding processes while closing tubes ends. It depends on deforming a rotating tube using a roller, and therefore, it is also called tube end spinning. The process involves many parameters like contact depth, roller inclination angle, roller diameter, mandrel curvature, and tube rotational speed. This study develops a finite element model (FE-model) for this process and validates it through experimental results. The numerical and experimental results have shown minor deviation of 1.87%. The FE-model is then employed to carry out a statistical analysis based on the response surface method (RSM). The analysis of variance (ANOVA) and regression analysis have proved the accuracy of the obtained mathematical model. The contact depth has proved to have the most significant effect in the process responses, while the roller diameter has the least effect. Finally, an optimization analysis is carried out to select the finest conditions for the process.

1. Introduction

Metal forming technology has proved over decades; it is the backbone of an enormous range of industries. There are countless applications involved in this field, such as deep drawing, blanking, coining, hydroforming, die forming, spinning, and tube forming. There are various topics that serve the technology of metal forming such as plasticity, forming limits, yield and failure criteria, strain rate, die design, lubrication, and process simulation [1]. In this study, tube end closing process, which is one of the essential metal forming applications, is targeted. A schematic illustration for the tube end closing process is presented in Figure 1. As shown in the figure, the basic principle of the process is to deform the end of the tube by sliding a roller towards the tube while it rotates, which makes it similar to metal spinning.

The greatest merit of the tube end closing is that it replaces the welding processes for closing the tube ends, which makes it classified as a clean production process. The concept of clean production has attracted many research institutions over the last decades. One of the valuable researches that have focused on the environmental effects of welding processes is introduced by [2]. The hazards on the respiratory, visual, and nervous human systems that are caused by the carcinogenic emissions of welding processes have been clarified. Moreover, as tubes have many applications in the medical industries, using welding processes in this case is almost prohibited. The purpose of this research work is to investigate the parameters involved in the tube end closing process, develop a validated FE-model, and perform a statistical and optimization analysis to find the finest process conditions. Following are summary of selected research works that have covered similar tube forming applications and others that have introduced similar optimization analyses.

Free bending of tubes is one of the recent topics of interest. Murata and Kuboki [3] have employed the computerized numerical control (CNC) to produce bent tubes based on the method of section (MOS). As the bending die is controlled by a CNC, the bending radius and bend direction can be flexibly

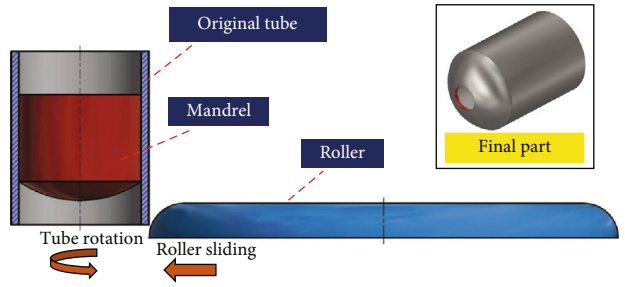

Figure 1: Basic idea of tube end closing process.

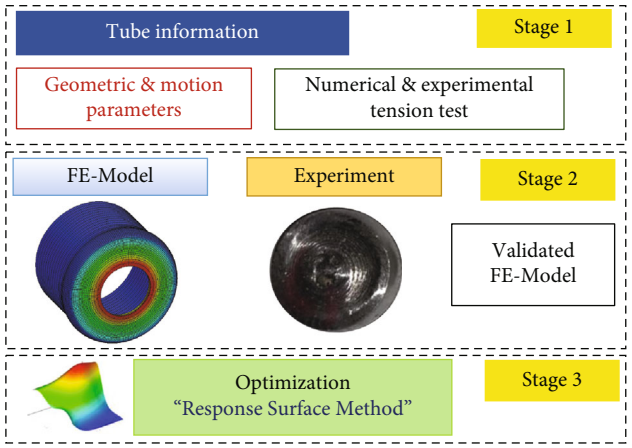

Figure 2: Structure of the research work.

adjusted. The benefits of the process and its applications have been clearly demonstrated. In the same context, simulation and experimental analysis of the tube free bending have been introduced by Guo et al. [4]. The distribution of the equivalent plastic strain (ϵ_p) on both the tube and the bending die has been analyzed throughout the different stages of bending. Moreover, the influence of process input parameters, such as clearance between tube and die, fillet radius of the guide, and feeding speed, has been investigated. In addition, another approach for tube end forming has been introduced by Tkachov et al. [5]. Small high-pressure cylinders have been produced using the swaging process with the aid of preheating to accelerate deforming the end of the tube to the desired shape. The preheating has been controlled using a two-layer inductor, and lubricants have been tested to obtain high-quality products. Moreover, another application of the tube end forming has been proposed by Alves et al. [6]. The tube end forming has been employed to join the tube to a sheet panel without any need for welding or riveting. Numerical and experimental modeling of the process has been established, and the proposed joining method has proved feasible. Besides, one of the essential disciplines in the field of metal forming in general is the forming limit. Magrinho et al. [7] have introduced a pioneer study of the determination of forming limits in thin-walled tubes. A method called digital image correlation (DIC) has been employed to predict the onset of failure by necking and also predict the corresponding strain limits. The study is considered a breakthrough

Table 1: Geometric input parameters of the tube end closing process.

Symbol	Description
α	Roller inclination angle
ε	Depth of contact at $\alpha = 0$, measured from tube's face [mm]
ε'	Depth of contact at $\alpha \neq 0$, measured from tube's face [mm]
ε_m	Depth of the mandrel measured from tube's face [mm]
C	Center distance between roller and tube for $\alpha = 0$ [mm]
C'	Inclined center distance between inclined roller and tube for $\alpha \neq 0$ [mm]
d_i	Inner tube diameter [mm]
d_o	Outer tube diameter [mm]
d_r	Roller diameter [mm]
d_m	Mandrel diameter [mm]
t_i	Initial tube thickness [mm]
r_m	Radius of mandrel's curvature/fillet [mm]
d_f	Tube closing diameter of the final deformed tube [mm]

and is expected to contribute to the future of tube forming processes.

On the other hand, optimization techniques have been employed to find the optimum conditions of the metal forming process that satisfies a specific objective function. Wang et al. [8] have introduced a detailed state-of-the-art that is considered a useful guide for the researchers who are interested in this field. Popular software and the surrogate model used in each one are presented. Along the same lines, Karagöz and Yıldız [9] have compared between various metaheuristic algorithms, yet for the crashworthiness of vehicle thin-walled tube structures. The metaheuristic algorithms are optimization techniques that are designed based on observed natural phenomena, such as the gravitational search algorithm (GSA) and bat algorithm (BAT). Nine algorithms have been tested while studying the effect of metal forming process parameters on the performance of the thin-walled structure. The hybrid GSA algorithm has shown the best results. In the same vein, a comprehensive study has been introduced by Keshtiara et al. [10] in the field of laser forming. The laser beam has been employed to bend the tubes and the laser beam parameters have been investigated. A FE-model of the process has been developed using ABAQUS, and hence, the Taguchi design of experiment has been used for the statistical analysis. Finally, a multiobjective optimization analysis has been carried out using a genetic algorithm (GA) to find the global optimum condition.

Based on the literature, it is revealed that a statistical analysis of the parameters affecting the tube end closing process is not sufficiently covered. Therefore, this study aims first to develop a FE-model that can realistically simulate the real-life process. This can be achieved by validating the numerical results, specifically the tube closing diameter, to those obtained experimentally. The analysis is carried out on a standard size tube having an outer diameter of 31.75 mm

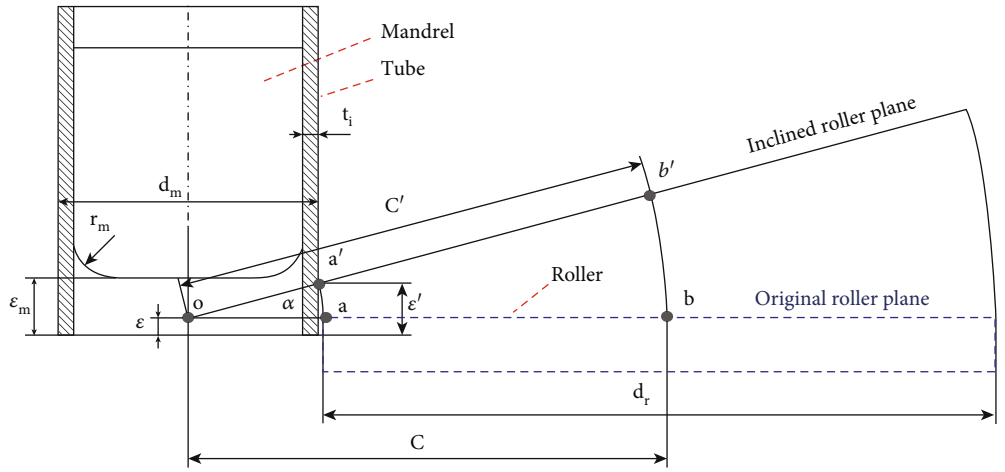

Figure 3: Geometric parameters involved in tube end closing process.

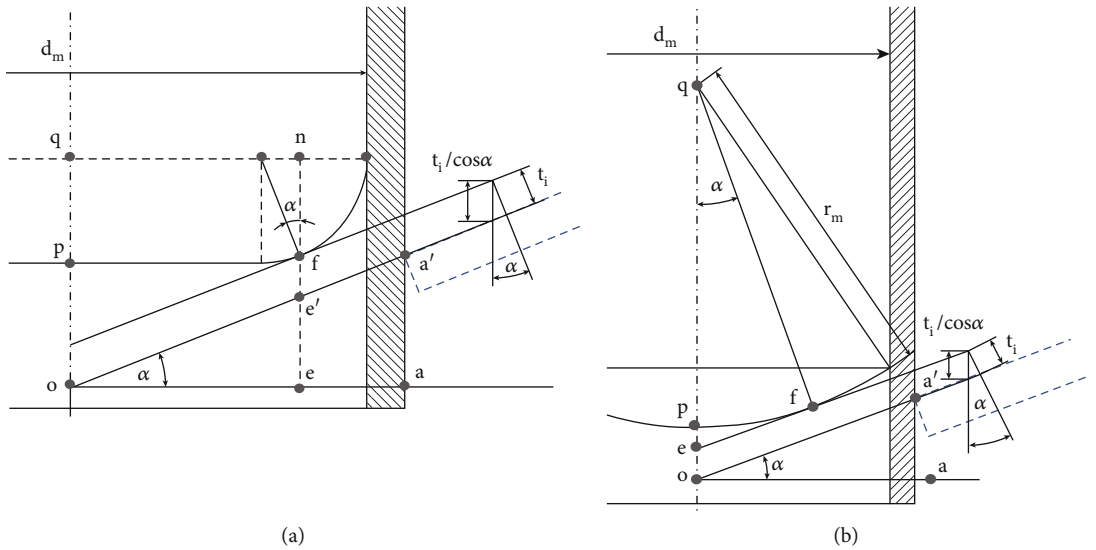

Figure 4: Determination of mandrel position for (a) mandrel design 1 and (b) mandrel design 2.

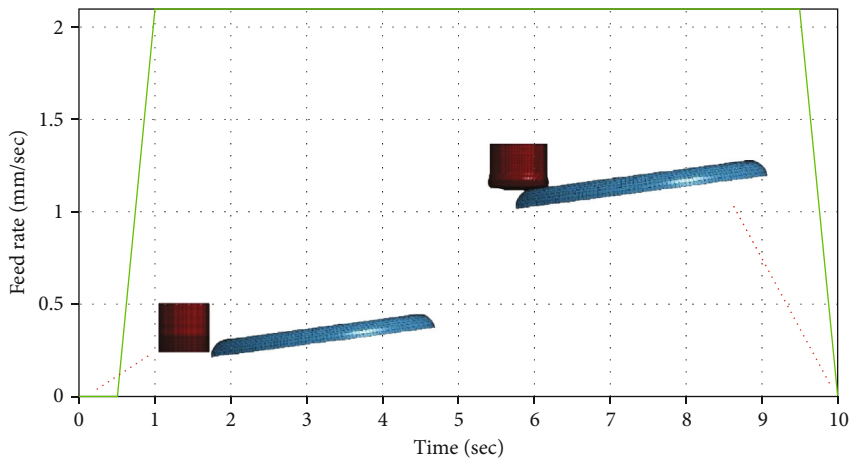

Figure 5: Feed rate of the roller throughout the tube end closing process.

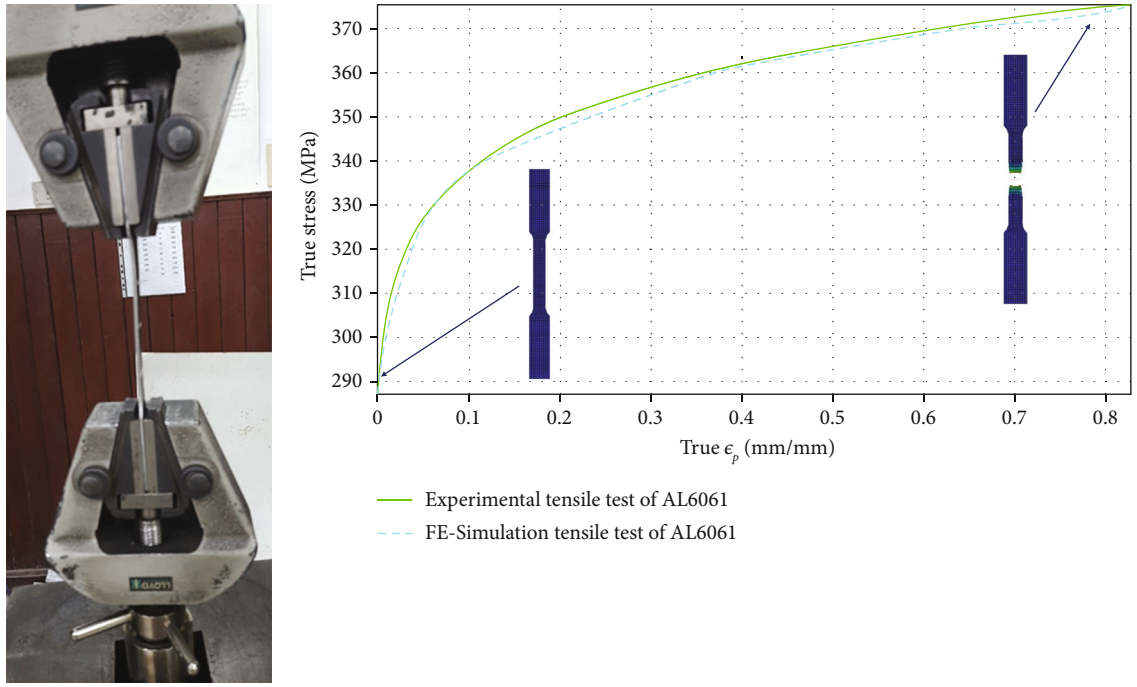

(a) (b)

Figure 6: True stress and true ϵ_p obtained from experimental and numerical tensile tests.

Table 2: Properties of AL6061-T6-T6 as obtained from tensile test.

Young's modulus (E)	Elongation to failure	Yield stress (σ_y)	Ultimate stress (σ_u)	Poisson's ratio (υ)
68.94 GPa	13%	287 MPa	370 MPa	0.3

and thickness of 1.778 mm and manufactured out of AL6061-T6. Moreover, this study introduces a statistical analysis to study the effect of various input parameters such as contact depth, roller inclination angle, roller diameter, mandrel curvature, and tube rotational speed. The selected responses for the analysis are the tube closing diameter and the resultant load. Besides, in this study, the response surface method (RSM) is used to develop a surrogate model that can replace the original numerical model. Analysis of variance (ANOVA) and regression analysis are carried out to evaluate the accuracy of the mathematical model. Finally, this study introduces an optimization analysis for the tube end closing by which the finest process conditions can be determined.

The structure of the research work is as follows: (1) the principles of the tube end closing process are investigated, (2) the FE-model is developed, (3) the numerical results are presented, (4) the tube end closing experiment is carried out and the numerical and experimental results are compared to each other, and (5) a statistical and optimization analysis of the process is carried out. The structure of the research work is illustrated in Figure 2.

2. Tube End Closing Principles

Similar to the metal spinning process, the tube end closing depends mainly on moving a free rotating roller linearly towards a rotating tube supported by an inner mandrel. The process is categorized as one of the tube end forming processes, which depends on deforming the end of the tube into a desired shape rather than using caps and welding. By definition, the purpose of the tube end closing process is to convert the open end of a tube into a closed end, yet with a predefined closing diameter. Hence, it is required to decide the proper process parameters that can purposely result in closing the diameter of the tube as desired. Accordingly, this section is concerned with defining the parameters involved in the tube end closing process, which paves the way for further numerical analysis. The parameters of interest are divided into three categories: geometric, motion, and material parameters.

2.1. Geometric Parameters. The geometric parameters can be classified into fixed and variable parameters. The fixed parameters are those related to the manufacturing of tube, roller, and mandrel. Hence, they cannot be changed after manufacturing. As an example, parameters such as tube outer diameter (d_o), tube initial thickness (t_i), roller diameter (d_r), and mandrel curvature (r_m) are all considered fixed. On the other hand, the variable parameters are those related to the process settings. They can usually be adjusted on the machine upon which the tube end closing process is carried out, such as contact depth (ε'), roller inclination angle (α),

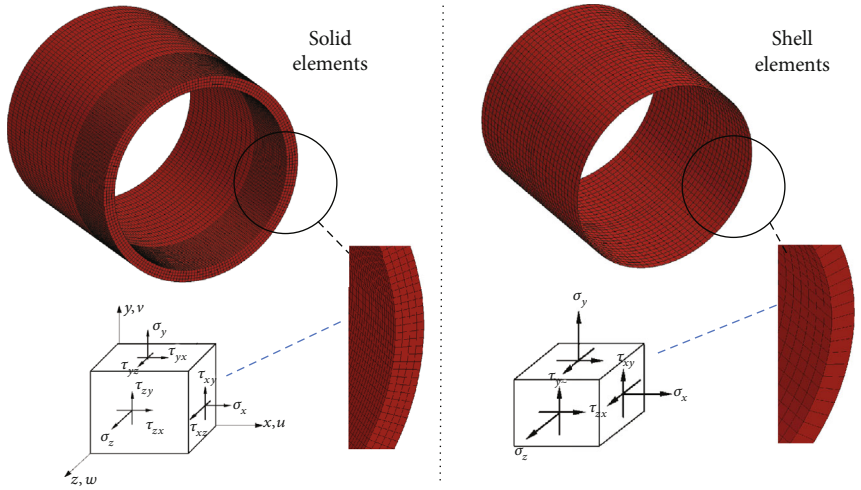

Figure 7: Comparison of solid and shell elements for modeling the tube.

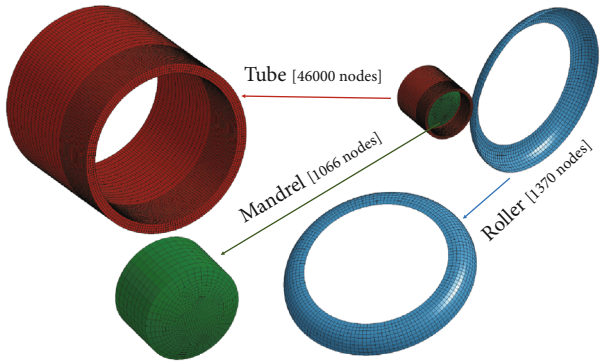

Figure 8: Meshing of tube, roller, and mandrel using LS-Dyna©.

and the mandrel depth (ε_m). The main geometric parameters involved in the process are defined in Table 1.

The contact depth (ε') is the fundamental variable parameter based on which all other variable parameters are decided. Figure 3 shows the dependency of the roller position on the contact depth (ε') and the effect of the roller inclination angle (α) as well. The general position of a roller inclined by an angle α can be defined in terms of center distance (C'), and contact depth (ε), which is the contact depth at $\alpha = 0$, as shown in the following equations:

$$\varepsilon = \varepsilon' - \frac{d_o}{2} \tan \alpha, \tag{1}$$

$$C' = \frac{d_o}{2 \cos \alpha} + \frac{d_r}{2}. \tag{2}$$

As shown in Figure 3, the position of the roller is first defined within the original roller plane ($\alpha = 0$) by defining the contact depth (ε), which is the offset of point (a) from the tube's face. Then, the original plane is transformed by an angle α about point (o) to the inclined roller plane. The desired contact depth (ε') is defined based on the point (a'), which is the actual contact point between tube and roller.

On the other hand, the offset of the mandrel from the tube's face (ε_m) should be controlled so that it provides inner support for the tube against the undesired forms of deformations, while considering the tube thickness throughout the process. Figures 4(a) and 4(b) show two different mandrel designs, while the mandrel depth (ε_m) for each case is determined from the following equations:

$$\textbf{Mandrel (1)}: \varepsilon_m = \varepsilon + r_m(\cos \alpha - \tan \alpha + \tan \alpha \sin \alpha - 1) + \frac{d_m}{2} \tan \alpha + \frac{t_i}{\cos \alpha}, \tag{3}$$

$$\textbf{Mandrel (2)}: \varepsilon_m = \varepsilon + \frac{t_i + r_m(1 - cos\alpha)}{\cos \alpha} \tag{4}$$

From the equations, it can be noticed that the mandrel depth (ε_m) is function of contact depth (ε), mandrel curvature (r_m), roller inclination angle (α), and the tube thickness (t_i).

2.2. Motion Parameters. There are two basic motions involved in the tube end closing process: the tube rotation and the roller translation. Similar to metal spinning process, the tube end closing can be executed on a turning machine by simply holding the tube to the spindle and mounting the roller attachment to the carriage. One of the interests of this research work is to study the effect of the tube rotational speed (N) on various process responses. On the other hand, the feed rate of the roller should be adjusted at an intermediate value (2.1 mm/sec) to prevent high strain rates. The distance travelled by the roller throughout the process must guarantee that the roller exceeds the tube center. It also should be considered that the roller starts to deform the tube only after the tube reaching the desired rotational speed. The feed rate of the roller throughout the tube end closing process is presented in Figure 5.

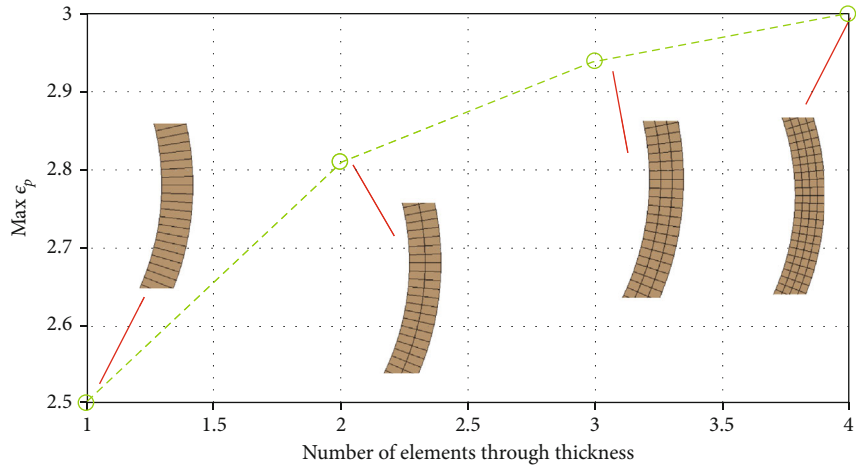

FIGURE 9: Effect of number of elements through tube thickness on the max ϵ_p.

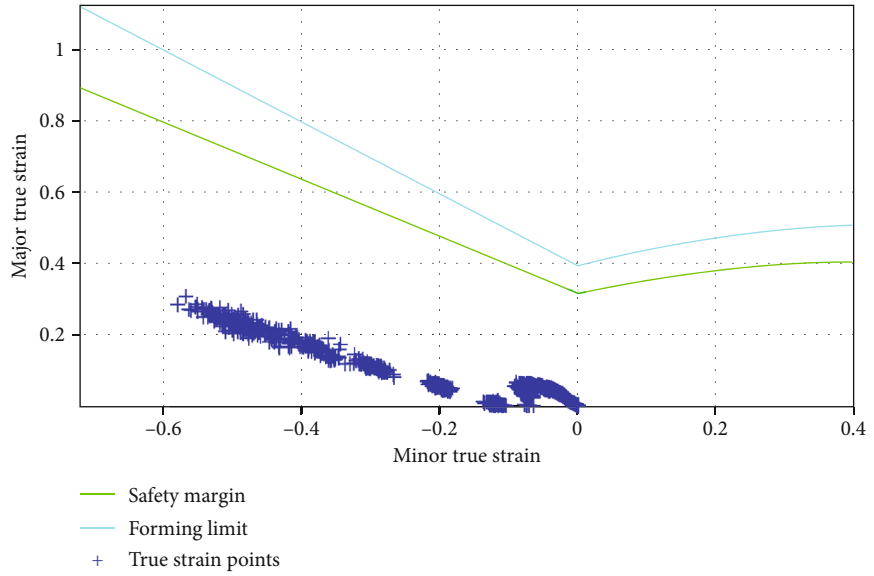

FIGURE 10: Forming limit curve, the safety margin curve, and the strain path for the tube end closing process.

2.3. Material Properties of AL6061-T6. The properties of the tube material are undoubtedly one of the basic parameters that influence the tube end closing process. Obtaining the properties of AL6061-T6 is essential to provide the FE-solver with the material information required for the numerical analysis. Therefore, an experimental tensile test is carried out on a standard specimen out of an AL6061-T6 alloy as shown in Figure 6(a). The experimental tensile test has been repeated three times for three specimens. The results represented in Young's Modulus (E), yield stress (σ_y), and ultimate stress (σ_u) are shown in Table 2.

However, the FE-solver only accepts true effective stress and true equivalent plastic strain (ϵ_p) values [11]. Consequently, the experimental data is transformed to fulfill this requirement, and finally, the plasticity characteristics of AL6061-T6 are defined. For validation, an explicit analysis for the tensile test is carried out on LS-Dyna 4.3© using the piecewise linear plasticity model (MAT_024) material model, and the generated results are compared to those obtained experimentally. The similarity of the numerical and experimental results shown in Figure 6(b) proves the accuracy of the material model.

3. Developing FE-Model using LS-DYNA©

3.1. Principle of Numerical Analysis. Studying the complicated mechanics involved in tube end closing process analytically is insufficient. Moreover, experimental technique is also limited because of the presence of multiple parameters that influence the process, which makes studying the process each time a parameter changes very costly. Instead, a FE-model that can accurately simulate the real-life process can provide an efficient tool for study. In this section, the FE-model of the tube end closing is developed using LS-Dyna

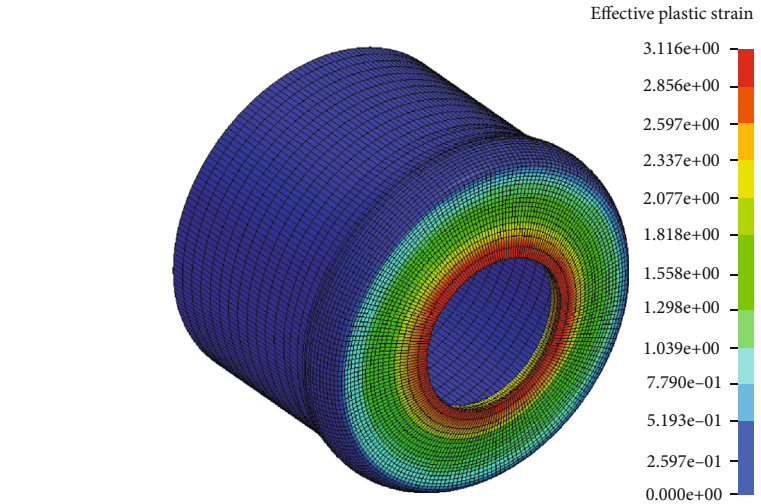

(a)

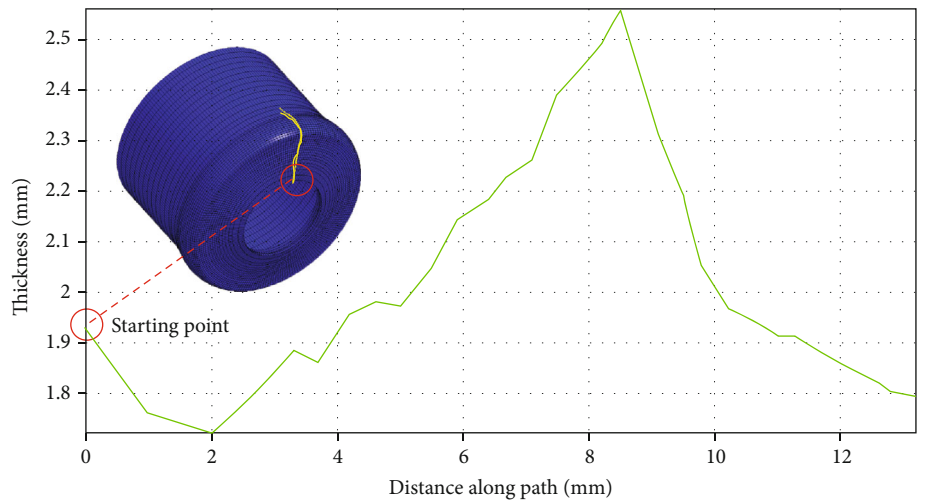

(b)

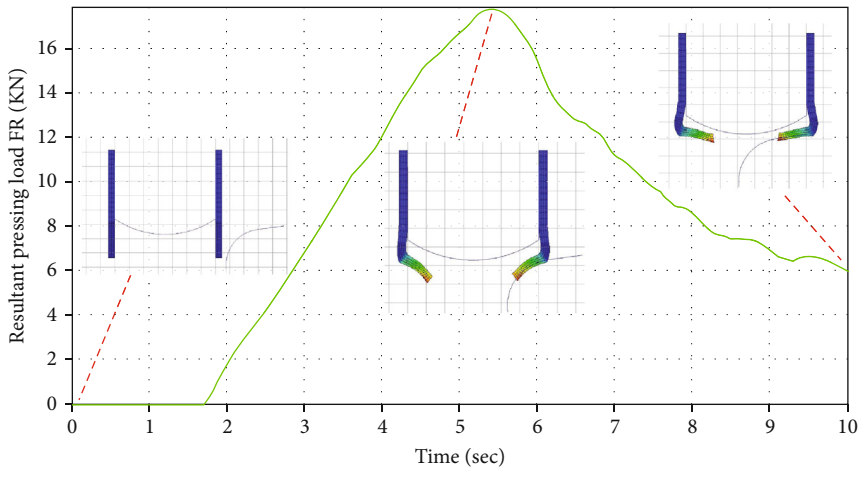

(c)

Figure 11: Continued.

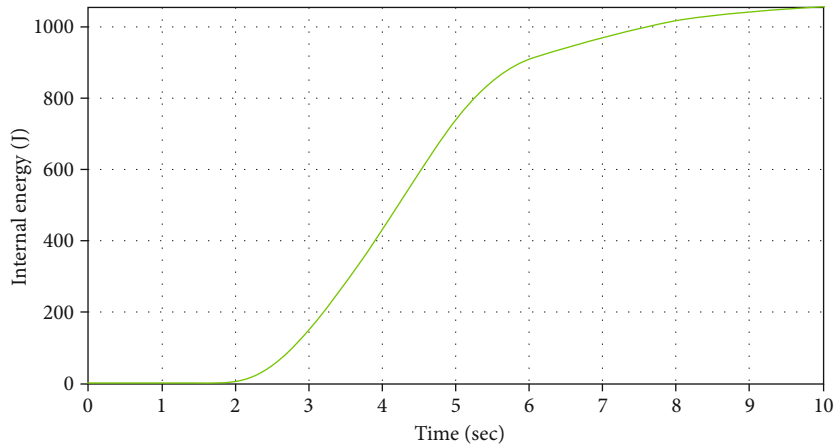

(d)

Figure 11: Results obtained from the numerical simulation. (a) Distribution of equivalent plastic strain ϵ_p. (b) Thickness along an imaginary path. (c) Resultant pressing load. (d) Internal energy of the deformed tube, under the following conditions [$\varepsilon' = 6.5$ mm, $\alpha = 7.5°$, $r_m = 50$ mm, $d_r = 140$ mm, and $N = 800$ rpm].

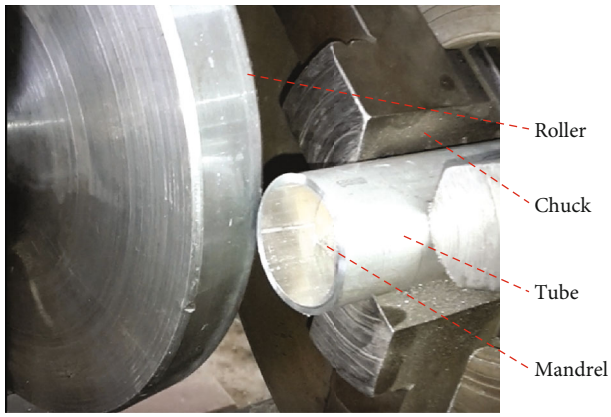

Figure 12: Experimental setup of the tube end closing process.

4.3©. Basic items involved in developing the FE-model, such as mesh settings, material modeling, and boundary conditions, are all discussed.

3.2. Mesh Settings. As the material behaviour in the tube end closing process is extremely nonlinear, the explicit dynamic analysis is employed. Generally, the time step for explicit analyses depends mainly on the mesh quality. On other words, the least local time step usually corresponds to the element of the least quality, and in turn, the global time step of the system is limited to this value [12]. Based on all above,

Based on all above, as the stress variation through the tube thickness cannot be considered negligible, solid elements are selected to model the tube. As the end of the tube is the region exposed to the highest deformation, it is modeled using a finer mesh size. Moreover, the circumference of the tube is divided into 100 divisions to obtain a mapped mesh of solid quadrilateral elements. The tube thickness is divided into 4 elements after a mesh-independent test is carried out as discussed later. The meshing of tube, roller, and mandrel is presented in Figure 8.

selecting the suitable element type with the proper mesh size and aspect ratio is essentially claimed. From this aspect, the tube is the critical part as it is the only deformable one, while the roller and mandrel are assumed to be rigid. Being rigid, shell elements are undoubtedly suitable to model both roller and mandrel to minimize the model size. However, the decision to use shell or solid elements to model the tube needs a brief study of the nature of both element types, and how suitable each one is to the case of the tube.

In general, shell elements are suitable for cases of plane stress (membrane stress), which makes them the common choice for most of metal forming process simulations. As shown in [5], the plane stress is the case when any stress component related to local z-direction is considered zero, which makes the model size relatively low. Where the normal and shear stresses in the equation are denoted by (σ) and (τ), respectively. For isotropic materials, the constitutive equation showing the stress-strain relation in case of plane stress is shown in [6, 13]. Where the normal and shear strains are denoted by (ϵ) and (γ), respectively. In other words, shell elements are suitable in case the through-thickness variations are not of interest. On the other hand, the capacity of solid elements is unlimited as the six independent stress components are all considered within the constitutive equation as shown in [7]. A comparison of using shell and solid elements for modeling the tube is shown in Figure 7.

3.3. Material Models. In the previous section, the properties of AL6061-T6 are obtained experimentally, and the data is transformed to suit the standards of the FE-solvers. This data is then used to provide the selected material model for the tube, which is the piecewise linear plasticity model (MAT_024), with all material data required such as density, young's modulus, Poisson's ratio, yield stress, and the isotropic hardening curve. It should be noted that the failure criteria available in this material model is only suitable for cases of uniaxial tension, which is not the case of this study. Instead,

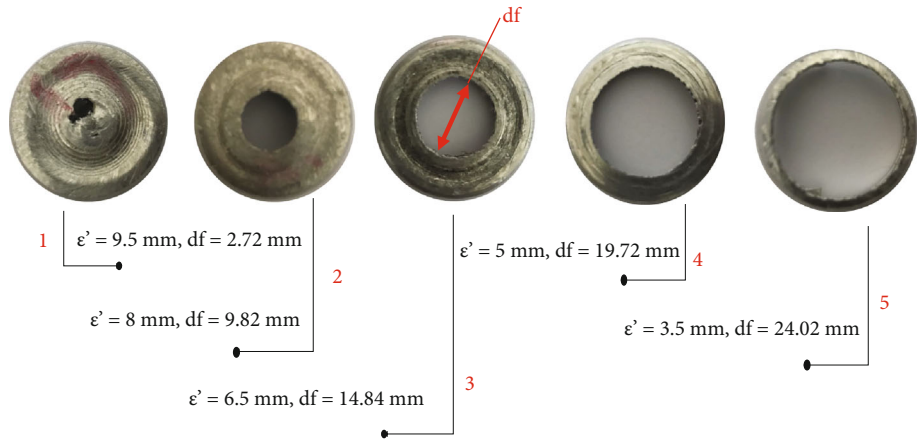

FIGURE 13: Deformed tubes obtained by five experiments each carried out at a specific contact depth while keeping the rest of parameters the same [$\alpha = 7.5°$, $r_m = 50$ mm, $d_r = 140$ mm, and $N = 800$ rpm].

$$\sigma_z = \tau_{yz} = \tau_{xz} = 0, \tag{5}$$

$$\begin{Bmatrix} \sigma_x \\ \sigma_y \\ \tau_{xy} \end{Bmatrix} = \frac{E}{(1+\upsilon)(1-2\upsilon)} \begin{bmatrix} 1-\upsilon & 0 & 0 \\ 0 & 1-\upsilon & 0 \\ 0 & 0 & (1-2\upsilon)/2 \end{bmatrix} \begin{Bmatrix} \epsilon_x \\ \epsilon_y \\ \gamma_{xy} \end{Bmatrix}, \tag{6}$$

$$\begin{Bmatrix} \sigma_x \\ \sigma_y \\ \sigma_z \\ \tau_{xy} \\ \tau_{yz} \\ \tau_{xz} \end{Bmatrix} = \frac{E}{(1+\upsilon)(1-2\upsilon)} \begin{bmatrix} 1-\upsilon & \upsilon & \upsilon & 0 & 0 & 0 \\ \upsilon & 1-\upsilon & \upsilon & 0 & 0 & 0 \\ \upsilon & \upsilon & 1-\upsilon & 0 & 0 & 0 \\ 0 & 0 & 0 & (1-2\upsilon)/2 & 0 & 0 \\ 0 & 0 & 0 & 0 & (1-2\upsilon)/2 & 0 \\ 0 & 0 & 0 & 0 & 0 & (1-2\upsilon)/2 \end{bmatrix} \begin{Bmatrix} \epsilon_x \\ \epsilon_y \\ \epsilon_z \\ \gamma_{xy} \\ \gamma_{yz} \\ \gamma_{xz} \end{Bmatrix}. \tag{7}$$

the localised necking criteria are employed to obtain the forming limit diagram FLD, as discussed later.

3.4. Boundary Settings. As both mandrel and roller are assumed rigid, the material model (MAT_RIGID) is found adequate as suggested by Maker and Zhu [14]. This material model provides defining the degrees of freedom of the part with respect to the global coordinates. Hence, the mandrel is set to be only allowed to rotate about z-axis. On the contrary, the degrees of freedom of the roller cannot be defined with respect to the global coordinates, as it is inclined in some cases. Instead, the roller is set to be only allowed to move translationally with respect to a vector, which is predefined based on the inclination angle. The rotational speed of the mandrel, which is the same for the tube, together with the translational motion of the roller, is both defined as rigid body motions using the (BOUNDARY_PRESCRIBED_MOTION_RIGID) based on the data previously obtained in Section 2. On the other hand, the boundary settings for the tube should consider the following: (1) the tube is free to rotate about z-axis, (2) the displacement of the nodes within the xy-plane is permitted to allow the deformation, and (3) the translation of the tube as a rigid body in x or y -axis is prohibited. These three conditions have been successfully satisfied using (PRESCRIBED_MOTION_SET) and (SPC_SET). Finally, the contact settings between the roller and the tube have been defined using (FORMING_ONE_WAY) with sliding option enabled and 0.2 coefficient of friction.

4. Finite Element Analysis Results

4.1. Effect of through Thickness Mesh Size. The larger the number of elements through the tube thickness, the more

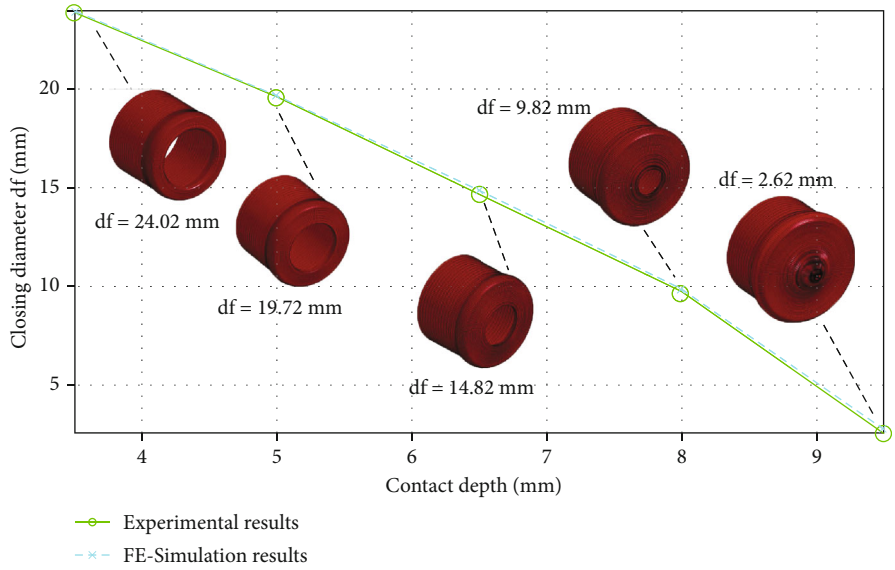

Figure 14: Numerical and experimental results of five experiments each carried out at a specific contact depth while keeping the rest of parameters the same [$\alpha = 7.5^{\circ}$, $r_m = 50$ mm, $d_r = 140$ mm, and $N = 800$ rpm].

Table 3: Comparison of numerical and experimental results of five experiments each carried out at a specific contact depth while keeping the rest of parameters the same [$\alpha = 7.5^{\circ}$, $r_m = 50$ mm, $d_r = 140$ mm, and $N = 800$ rpm].

Contact depth (ε')	Numerical d_f (mm)	Experimental d_f (mm)	Error%
9.5	2.48	2.62	5.34
8	9.62	9.82	2.04
6.5	14.66	14.82	1.08
5	19.62	19.72	0.51
3.5	23.92	24.02	0.42
			Average error% = 1.88

accurate the results, but also the larger the size of the model. To select the optimum number of elements through the tube thickness, a mesh-independent test has been carried out as shown in Figure 9. Generally, the mesh-independent test aims to check that the numerical simulation is only sensitive to the changes corresponding to the process being simulated, without any undesirable noise. The number of elements through the tube thickness is changed from 1 to 4, and the value of maximum ϵ_p is observed each time. As shown in Figure 9, the last two iterations show the maximum ϵ_p values of 2.94 and 3 which satisfies a convergence within only 2%. Hence, the FE-model is proved to be mesh-independent.

4.2. Forming Limit Diagram (FLD). To evaluate the tube end closing process, a failure criterion should be clearly defined. The variation of the state of stress makes it insufficient to depend on only one failure criterion [15]. Instead, the FLD, which is mainly a plot of the minor and major true strains, is employed as shown in the graph in Figure 10. In addition to the strain path, the FLD also contains a safety margin

Table 4: The design levels of the selected input variables.

Controllable variable	Notation	Unit	-1	0	1
Roller inclination angle	$\boldsymbol{\alpha}$	—	0	7.5	15
Depth of contact point between inclined roller and tube	$\boldsymbol{\varepsilon'}$	mm	3	6	9
Radius of mandrel's curvature/fillet	$\boldsymbol{r_m}$	mm	40	50	60
Roller diameter	$\boldsymbol{d_r}$	mm	100	140	180
Tube rotational speed	$\boldsymbol{N}$	rpm	400	800	1200

curve and a forming limit curve. In LS-Dyna©, those two curves are plotted based on the following: (1) the sheet thickness, which is 1.778 mm; (2) the material properties, specifically the hardening exponent, which is 0.235 for AL6061-T6. As the plots of major and minor strains are far away from the necking region, the tube end closing process is proved to be successful.

4.3. Numerical Results. The numerical simulation of the tube end closing process is carried out under the following conditions: [$\varepsilon' = 6.5$ mm, $\alpha = 7.5^{\circ}$, $r_m = 50$ mm, $d_r = 140$ mm, and $N = 800$ rpm] and the results are presented in Figures 11(a)–11(d). The maximum ϵ_p is recorded at the end of the tube as 3.11. Besides, the thickness distribution along a path at the end of the tube shows that the maximum thickness is 2.56 mm located at the round edge of the deformed tube, which indicates a thickening percentage of 44%. Moreover, the maximum resultant load generated at the contact point between roller and tube is 17.8 kN and occurs after 5.4 sec from the process start. Finally, the internal energy of the deformed tube reaches its maximum by the end of the process as it exceeds 1000 J. The internal energy is usually used to figure out the capacity needed for the machine upon which the metal

Table 5: Design table based on the DOE with the calculated results.

Test number	α	ε'	r_m	d_r	N	d_f	F_{Rmax}
1	-1	-1	-1	-1	1	30.95	7.24
2	1	-1	-1	-1	-1	25.25	7.64
3	-1	1	-1	-1	-1	5.95	34.1
4	1	1	-1	-1	1	5.72	26.16
5	-1	-1	1	-1	-1	26	10.4
6	1	-1	1	-1	1	26.44	7.42
7	-1	1	1	-1	1	10.24	24.5
8	1	1	1	-1	-1	6.34	31.97
9	-1	-1	-1	1	-1	25.77	10.49
10	1	-1	-1	1	1	26.74	7
11	-1	1	-1	1	1	10.84	23.5
12	1	1	-1	1	-1	6.32	31.6
13	-1	-1	1	1	1	30.46	7.74
14	1	-1	1	1	-1	25.03	7.77
15	-1	1	1	1	-1	6.03	35.1
16	1	1	1	1	1	5.06	28
17	-1	0	0	0	0	17.25	16.1
18	1	0	0	0	0	16.16	15.3
19	0	-1	0	0	0	25.86	8.27
20	0	1	0	0	0	4.6	29
21	0	0	-1	0	0	17.95	14.15
22	0	0	1	0	0	16.31	15.76
23	0	0	0	-1	0	16.48	15.54
24	0	0	0	1	0	16.42	15.78
25	0	0	0	0	-1	16.08	17.5
26	0	0	0	0	1	19.31	13.9
27	0	0	0	0	0	16.41	15.5

forming process is carried out. The numerical analysis is then repeated, yet at various depths of contact [3.5, 5, 8, and 9.5 mm], while holding the rest of input parameters the same. The results of those analyses are presented in the following section.

5. Experimental Procedure

5.1. Setup of Process Parameters. In this study, tube end closing process is executed experimentally on a turning machine. The tube and mandrel are both fixed to a three-jaw chuck, and the rotational speed is controlled by a DC motor, as is usually the case in turning operations. To control the contact depth and the feed rate of the roller, the roller is mounted to the carriage of the turning machine, but via a special attachment that permits the rotational motion. Besides, by attaching the roller to the carriage, the inclination angle of the roller can be controlled.

The roller is a disk shaped of 140 mm diameter and is manufactured out of steel K110 coated with nickel chrome to obtain a higher hardness for the outer surface. As for the tube, a 2 m long bar of tube is used, and the protruding part is renewed after each experiment. According to the tube standards, the tube is manufactured out of AL6061-T6 and has 31.75 mm outer diameter and 1.778 mm thickness. The protruding length of the tube outside the chuck is set to be 30 mm to eliminate the bending effect on the tube as much as possible. A lubricant is used to provide a smooth contact between the tube and the roller throughout the process. The experimental setup of the tube end closing process is shown in Figure 12.

5.2. Experimental Results. In this study, five experiments have been carried out each at different contact depths ε' while holding the rest of input parameters as follows: [$\alpha = 7.5°$, $r_m = 50$ mm, $d_r = 140$ mm, and $N = 800$ rpm]. The contact depth ε' is changed from 3.5 mm to 9.5 mm by step of 1.5 mm. The process response of interest in this study is the tube closing diameter d_f. The deformed tubes obtained from the five experiments are shown in Figure 13.

As the basic purpose of the experiments is to validate the FE-model results, the results of both numerical and experimental analyses are plotted against each other as shown in the graph in Figure 14. Besides, Table 3 presents the values of the tube closing diameter d_f corresponding to each contact depth. Finally, the validation of the FE-model is successful as the average error in the results is 1.87% which is within the accepted range.

6. Statistical Analysis

6.1. Principles of Statistical Analysis. In this section, a statistical analysis is carried out to study the parameters involved in the tube end closing process. Through previous sections, a validated FE-model that can simulate the real-life process has been developed successfully. Hence, this FE-model can be employed to analyze the effect of various input parameters on a set of process responses of interest. However, due to the presence of various input parameters, studying the relation between input and output variables using the FE-model is costly. Instead, a statistical method called response surface method (RSM) is used to develop a surrogate model that can replace the original one. This surrogate model is simply a mathematical relation that provides an approximation for the real relation between the independent input variables and the process responses within a minimum error. Hence, the solving process depends on substituting in the mathematical model instead of solving a complete finite element problem. The mathematical relation consists of three main terms: linear, quadratic, and interaction terms, as shown in [8].

$$y = \beta_o + \sum_{i=1}^{k} \beta_i x_i + \sum_{i=1}^{k} \beta_{ii} x_i^2 + \sum_i \sum_j \beta_{ij} x_i x_j, \tag{8}$$

where β_o is a constant value, β_i is the coefficient of the linear terms, β_{ii} is the coefficient of the quadratic terms, β_{ij} is the coefficient of the interaction terms, and k is the number of independent variables.

6.2. Design of Experiment. To create the desired mathematical relation, a design of experiment DOE is first carried out. DOE is used to create a set of experiments each has specific set of

Table 6: Regression table for tube closing diameter d_f and maximum resultant force F_{Rmax}.

Term	d_f			F_{Rmax}		
	Regression coefficient	T value	P value	Regression coefficient	T value	P value
Constant	16.520	79.31	≤0.001	15.4700	66.50	≤0.001
$\boldsymbol{\alpha}$	-1.135	-8.59	≤0.001	-0.3506	-2.38	0.034
$\boldsymbol{\varepsilon'}$	-10.078	-76.27	≤0.001	10.5533	71.51	≤0.001
$\boldsymbol{r_m}$	-0.199	-1.51	0.156	0.3767	2.55	0.024
$\boldsymbol{d_r}$	-0.039	-0.30	0.773	0.1117	0.76	0.463
N	1.277	9.66	≤0.001	-2.2839	-15.48	≤0.001
$\boldsymbol{\alpha} * \boldsymbol{\alpha}$	0.172	0.48	0.640	0.2338	0.58	0.569
$\boldsymbol{\varepsilon'} * \boldsymbol{\varepsilon'}$	-1.303	-3.64	0.003	3.1688	7.91	≤0.001
$\boldsymbol{r_m} * \boldsymbol{r_m}$	0.604	1.68	0.116	-0.5112	-1.28	0.224
$\boldsymbol{d_r} * \boldsymbol{d_r}$	-0.079	-0.22	0.828	0.1938	0.48	0.637
$N * N$	1.162	3.24	0.006	0.2338	0.58	0.569
$\boldsymbol{\alpha} * \boldsymbol{\varepsilon'}$	0.007	0.05	0.963	0.4106	2.62	0.021
$\boldsymbol{\alpha} * N$	-1.107	-7.90	≤0.001	1.0444	6.67	≤0.001
$\boldsymbol{\varepsilon'} * N$	-0.332	-2.37	0.034	-1.4819	-9.47	≤0.001
	$\boldsymbol{R^2}$ = 99.79%, $\boldsymbol{R_{adj}^2}$ = 99.57%			$\boldsymbol{R^2}$ = 99.77%, $\boldsymbol{R_{adj}^2}$ = 99.54%		

values for the controllable variables. There are two main methods for the DOE, the central composite design CCD and the Box-Behnken design BBD. In this study, the CCD is selected with face centered option and no replications, which means a total of 27 experiment to be solved. Although there may be many input parameters involved in the tube end closing process, in this analysis, only five parameters are chosen as the controllable variables, which are roller inclination angle (α), contact depth (ε'), mandrel curvature (r_m), roller diameter (d_r), and tube rotational speed (N). The design levels (Boundary levels) for each controllable variable are listed in Table 4.

The selected response variables in this study are the tube closing diameter d_f and the maximum resultant load F_{Rmax}. The design table is created using Minitab19©. It contains the 27 tests and the coded values of the controllable variables as shown in Table 5. It also shows the values of the response variables as obtained by solving the FE-model.

6.3. ANOVA. The results of the tests shown in Table 5 are analyzed using ANOVA. The purpose of ANOVA is to study how significant each of the input variables is to the response variables. Variables that have significant effects are classified as "effective variables," while those that have insignificant effects are ignored and eliminated from the model. The effectiveness of a term is specified by comparing its corresponding "P value" to the "confidence level," which is usually 0.05. The confidence level indicates the maximum allowable error in a result predicted by the model. A term is considered effective if the "P value ≤ 0.05"; else, it is considered ineffective. The less the P value, the more significant the corresponding term. Moreover, the T values give another indication for the significance. The greater the absolute value of the T value, the more significant the corresponding term [16]. The sign of the T value also indicates whether the relation between a term and the response variable is direct or inverse. Table 6 represents the regression coefficients, T values, and P values for each term for both responses d_f and F_{Rmax}.

From the table, the following can be revealed:

As for the response variable d_f:

(i) The effective variables include the linear terms [$\alpha, \varepsilon', r_m$, and N], the quadratic terms [$\varepsilon'^2, r_m{}^2, N^2$], and the interactional terms [$\alpha N, \varepsilon' N$]. The rest of the terms are considered ineffective

(ii) All linear terms are inversely proportional to the response d_f except the term N

(iii) The linear term ε' has the most significant effect on the response d_f, while the term r_m has the least significant effect among all effective variables

As for the response variable F_{Rmax}:

(i) The effective variables include all the linear terms, the quadratic terms [$\varepsilon'^2, r_m{}^2$], and all the interactional terms. The rest of the terms are considered ineffective

(ii) All linear terms are directly proportional to the response F_{Rmax} except the terms α and N

(iii) The linear term ε' has the most significant effect on the response F_{Rmax}, while the term $r_m{}^2$ has the least significant effect among all effective variables

The correlation coefficients R^2 and $R_{\text{adj}}{}^2$ show a peak value of about 99% for both response variables as shown in the last row in Table 6. This indicates a high accuracy for

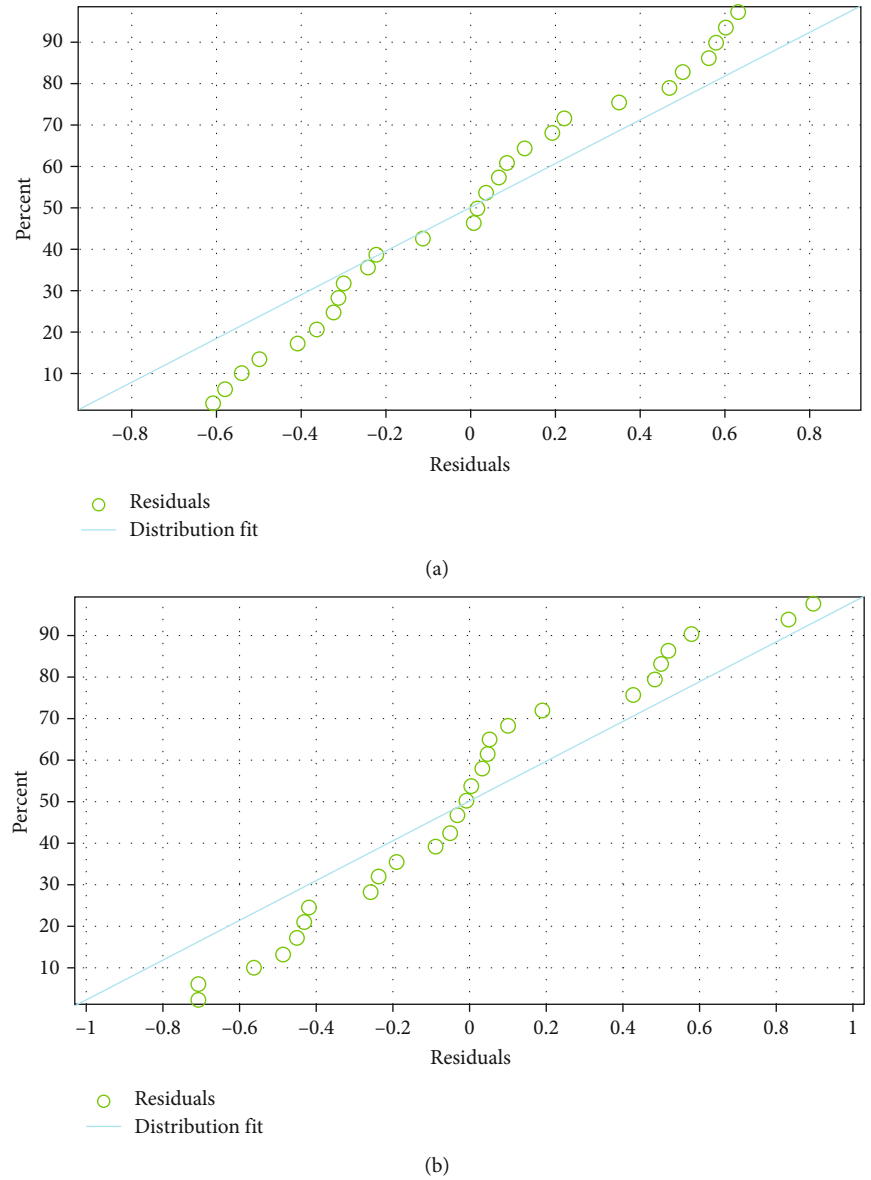

Figure 15: Normal probability plot for the data of (a) d_f and (b) F_R.

the regression model; however, more investigations are required for more confirmation.

From the normal probability plot shown in Figure 15, it can be noticed that the residuals follow a straight line for both responses d_f and F_{Rmax} and no divergence is noticed. In addition, the residual plots shown in Figure 16 show a normal distribution for the residuals around the zero axis and do not show any specific pattern. Based on all above, the obtained regression model is proved accurate and, hence, can be employed to obtain results instead of solving a complete finite element problem.

The relation between a specific response variable and two input variables can be presented in a 3D plot called "response surface" or 2D plots called "contour plots," while holding the other input variables at fixed values. The response surfaces and contour plots for both responses d_f and F_{Rmax} versus the contact depth ε' and the roller inclination angle α are shown in Figures 17(a), 17(b), 18(a), and 18(b), respectively, while the rest of input variables are fixed to the following values: [$r_m = 50$ mm, $d_r = 140$ mm, and $N = 800$ rpm].

7. Optimization Analysis

In this section, the mathematical model previously developed based on the RSM is employed to perform an optimization analysis. The purpose of an optimization analysis is to determine the optimal input variables that satisfy a specific objective function without violating a predefined set of constraints. There are various optimization techniques that have been employed in many previous researches. For example, the genetic algorithm (GA) and artificial neural network (ANN) were employed by Suresh et al. [17] to optimize the parameters affecting the surface roughness in the

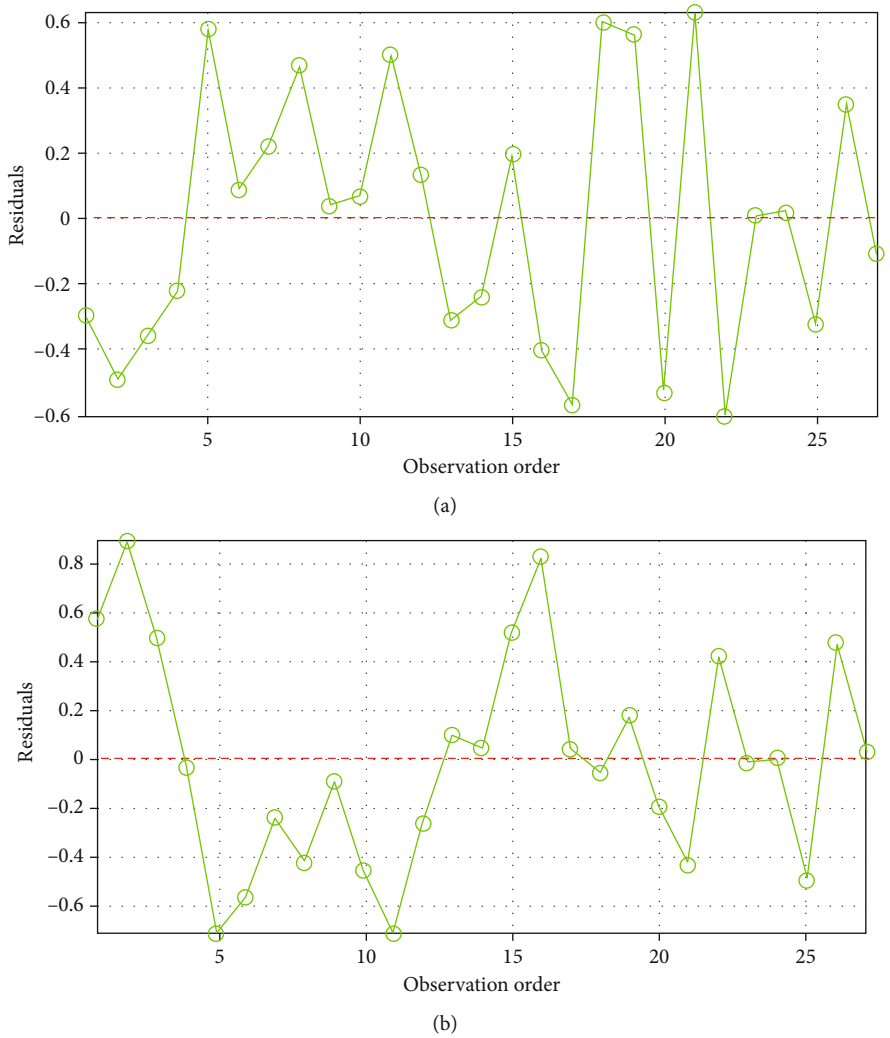

Figure 16: Residual plot for the data of (a) d_f and (b) F_R.

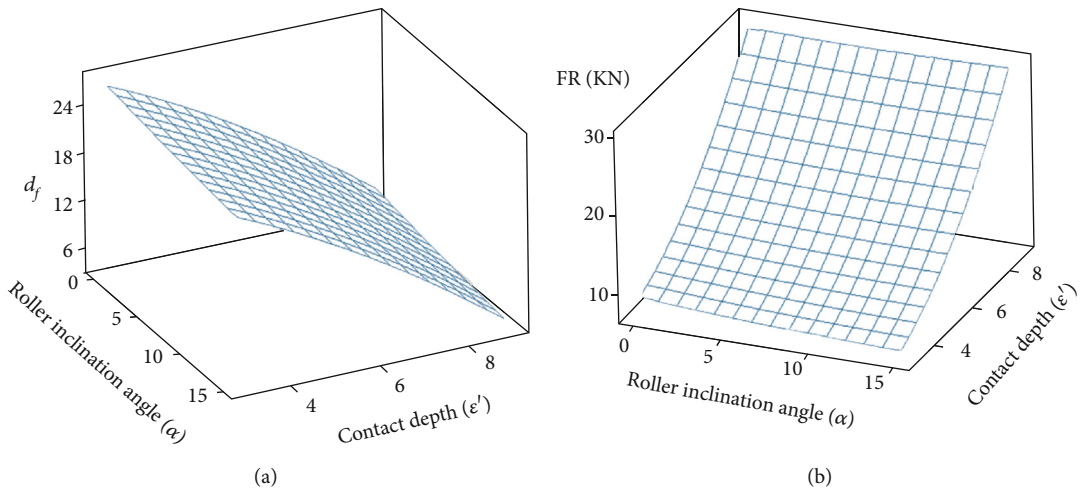

Figure 17: Response surfaces for (a) d_f and (b) F_R against roller inclination angle and contact depth, while holding the other input variable [r_m = 50 mm, d_r = 140 mm, and N = 800 rpm].

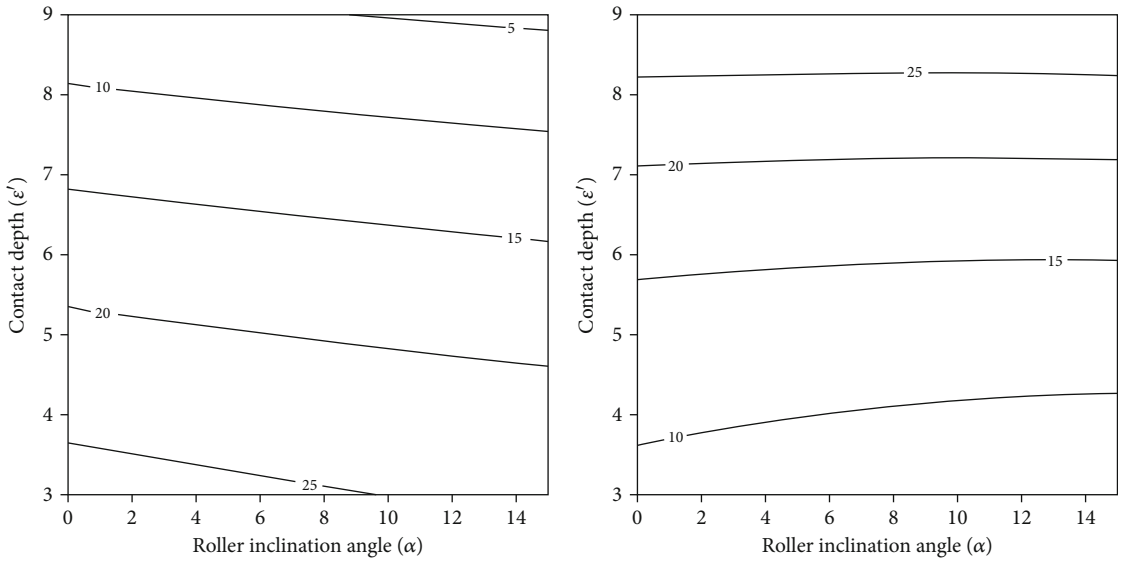

Figure 18: Contour plots for (a) d_f and (b) F_R against roller inclination angle and contact depth, while holding the other input variable [r_m = 50 mm, d_r = 140 mm, and N = 800 rpm].

Table 7: Optimal values of the input variables based on the defined constraints and objective functions.

Input variables	Constraint type	Uncoded values	Case (1) Minimize d_f	Case (2) Minimize d_f and F_{Rmax}
			Optimal values	
$\boldsymbol{\alpha}$	Constrain to region	[0 : 15]	15°	15°
$\boldsymbol{\varepsilon'}$ (mm)	Constrain to region	[3 : 9]	9	6.57
$\boldsymbol{r_m}$ (mm)	Hold value	50	50	50
$\boldsymbol{d_r}$ (mm)	Hold value	140	140	140
$\boldsymbol{N}$ (rpm)	Constrain to region	[400 : 1200]	828	990

Table 8: Comparison between the results obtained from the original FE-model and from the optimization analysis.

Case no.	Input variables					d_f (mm)			F_{Rmax} (kN)		
	α	ε' (mm)	r_m (mm)	d_r (mm)	N (rpm)	Conf. test	Optimization result	Error%	Conf. test	Optimization result	Error%
1	15°	9	50	140	828	4.25	4.17	1.9%	29.3	30.9	5.2%
2	15°	6.5	50	140	990	14.6	13.88	5.2%	16.87	16.9	0.17%

incremental forming process. However, in this study, the desirability method available in Minitab19© is employed.

The optimization analysis is performed twice: first, when the objective function is to minimize d_f only, and second, when the objective function is to minimize both d_f and F_{Rmax} simultaneously. For both cases, lower and upper limits are assigned to roller inclination angle (α) contact depth (ε'), and tube rotational speed (N), while the mandrel curvature radius (r_m) and the roller diameter (d_r) are considered hold values. Based on all the above, the optimal values for the input variables that satisfy each objective function are presented in Table 7.

To confirm the results of the optimization analysis, a confirmation test is carried out. Based on the optimal input variables, the original model, which is the previously developed FE-model, is used to obtain the tube closing diameter d_f and the maximum resultant load F_{Rmax}. The generated results of the FE-model are then compared to those determined by the regression model, and the differences are recorded as shown in Table 8. For case (1), the errors in d_f and F_{Rmax} are 1.9% and 5.2%, respectively, while for case (2), the same responses show errors of 5.2% and 0.17%, respectively. As the error percentages are within acceptable range, the optimization analysis is confirmed successfully.

8. Conclusion

In this study, the parameters involved in tube end closing process have been investigated. The tube end closing process is a metal forming process that is similar to metal spinning as it depends on deforming the tube by using a roller while the tube rotates. The tube upon which the analysis is carried out is manufactured out of AL6061-T6 and has 31.75 mm diameter and 1.778 mm thickness. Although there are many input parameters involved in the process, only five parameters are selected for this study, which are contact depth, roller inclination angle, roller diameter, mandrel curvature, and tube rotational speed. The principles related to the process have been studied and classified into three categories: geometric, motion, and material parameters. After that, the preprocessing setups required to develop the FE-model, such as meshing, material modeling, and boundary settings, have been all discussed. The results obtained by the FE-model under specific process conditions have been presented. In addition, the tube end closing process has been tested experimentally under the same process conditions. The numerical and experimental results have been compared to each other in terms of the tube closing diameter, and a minor deviation of only 1.87% has been recorded. Moreover, a statistical analysis has been carried out based on the response surface method (RSM). The central composite method (CCD) has been selected for the design of experiment (DOE), and a set of 27 tests has been established after selecting the upper and lower levels of the selected controllable variables. Based on the test results obtained by the FE-model, the regression model has been constructed. The correlation coefficients, the normal probability plots, and the residual plots have all proved the accuracy of the regression model. The contact depth has proved to have the most significant effect in the process responses, while the roller diameter has the least effect.

Finally, an optimization analysis has been carried out based on the desirability method. The analysis is aimed to find the finest conditions of the process that satisfy the objective function under two cases. For the first case, the objective function is to minimize the tube-closing diameter only. The finest process conditions have been found to be as follows: [contact depth: 9 mm, roller inclination angle: 15°, roller diameter: 140 mm, mandrel curvature: 50 mm, and tube rotational speed: 828 rpm]. On the other hand, the objective function in the second case is to minimize both the tube-closing diameter and the resultant load. The finest process conditions have been found to be as follows: [contact depth: 6.5 mm, roller inclination angle: 15°, roller diameter: 140 mm, mandrel curvature: 50 mm, and tube rotational speed: 990 rpm]. A confirmation test has been carried out to check the effectiveness of the optimization process. The results obtained from the original model have been compared to those obtained from the regression model and the difference percentages have been recorded. For case (1), the errors in d_f and F_{Rmax} are 1.9% and 5.2%, respectively, while for case (2), the same responses show errors of 5.2% and 0.17%, respectively. As the differences are within the acceptable range, the optimization analysis is confirmed successfully. For future work, the effects of other parameters such as the tube thickness, tube diameter, and the roller feed rate are suggested to be included in the analysis. Moreover, other optimization techniques can be tested.

Data Availability

The FE-Solver and the Optimizer working files that have been used to support the findings of this study are available from the corresponding author upon request.

Conflicts of Interest

The authors declare that they have no conflicts of interest.

References

[1] T. Altan and A. E. Tekkaya, Eds., *Sheet Metal Forming: Fundamentals*, ASM International, Ohio, 2012.

[2] F. Golbabaei and M. Khadem, "Air pollution in welding processes—assessment and control methods," in *Current air quality issues*, F. Nejadkoorki, Ed., pp. 33–63, IntechOpen, Croatia, 2015.

[3] M. Murata and T. Kuboki, "CNC tube forming method for manufacturing flexibly and 3-dimensionally bent tubes," in *60 excellent inventions in metal forming*, A. E. Tekkaya, W. Homberg, and A. Brosius, Eds., pp. 363–368, Springer-Verlag, Berlin, 2015.

[4] X. Guo, Y. Ma, W. Chen et al., "Simulation and experimental research of the free bending process of a spatial tube," *Journal of Materials Processing Technology*, vol. 255, pp. 137–149, 2018.

[5] R. O. Tkachov, V. V. Kukhar, E. S. Klimov, and A. H. Prysiazhnyi, "Development and application of tube end forming process with combined swaging and local differential preheating," *Materials Science Forum*, vol. 946, pp. 755–760, 2019.

[6] L. M. Alves, E. J. Dias, and P. A. F. Martins, "Joining sheet panels to thin-walled tubular profiles by tube end forming," *Journal of Cleaner Production*, vol. 19, no. 6-7, pp. 712–719, 2011.

[7] J. P. Magrinho, M. B. Silva, G. Centeno, F. Moedas, C. Vallellano, and P. A. F. Martins, "On the determination of forming limits in thin-walled tubes," *International Journal of Mechanical Sciences*, vol. 155, pp. 381–391, 2019.

[8] H. Wang, F. Ye, L. Chen, and E. Li, "Sheet metal forming optimization by using surrogate modeling techniques," *Chin J Mech Eng*, vol. 30, no. 1, pp. 22–36, 2017.

[9] S. Karagöz and A. R. Yıldız, "A comparison of recent metaheuristic algorithms for crashworthiness optimisation of vehicle thin-walled tubes considering sheet metal forming effects," *International Journal of Vehicle Design*, vol. 73, no. 1/2/3, pp. 179–188, 2017.

[10] M. Keshtiara, S. Golabi, and R. T. Esfahani, "Multi-objective optimization of stainless steel 304 tube laser forming process using GA," *Engineering with Computers*, vol. 37, no. 1, pp. 155–171, 2021.

[11] K. Suresh and S. P. Regalla, "Effect of mesh parameters in finite element simulation of single point incremental sheet forming process," *Procedia Materials Science*, vol. 6, pp. 376–382, 2014.

[12] A. P. Kumar and S. Shrivaathsav, "Influence of forming parameters on the crash performance of capped cylindrical

tubes using LS-DYNA follow-on simulations," *International Journal on Interactive Design and Manufacturing*, vol. 13, no. 3, pp. 1215–1232, 2019.

[13] D. V. Hutton, *Fundamentals of finite element analysis*, McGraw-Hill, New York, 2004.

[14] B. N. Maker and X. Zhu, "Input parameters for metal forming simulation using LS-DYNA," in *In: 6th international LS-DYNA conference*, Detroit, 2000.

[15] H. Chalal and F. Abed-Meraim, "Determination of forming limit diagrams based on ductile damage models and necking criteria," *Lat Am J Solids Struct*, vol. 14, no. 10, pp. 1872–1892, 2017.

[16] M. Vahdati, R. A. Mahdavinejad, and S. Amini, "Statistical analysis and optimization of factors affecting the spring-back phenomenon in UVaSPIF process using response surface methodology," *Int J Adv Des Manuf Technol*, vol. 8, pp. 13–23, 2015.

[17] K. Suresh, N. H. Rahman, S. P. Regalla, and A. K. Gupta, "Modeling and optimization of surface roughness in single point incremental forming process," *Journal of Materials Research and Technology*, vol. 4, pp. 304–313, 2015.